

Tailoring geometric phases of two-dimensional functional materials under light: a brief review

Jian Zhou

To cite this article: Jian Zhou (2020) Tailoring geometric phases of two-dimensional functional materials under light: a brief review, International Journal of Smart and Nano Materials, 11:3, 191-206, DOI: [10.1080/19475411.2020.1811796](https://doi.org/10.1080/19475411.2020.1811796)

To link to this article: <https://doi.org/10.1080/19475411.2020.1811796>



© 2020 The Author(s). Published by Informa UK Limited, trading as Taylor & Francis Group.



Published online: 26 Aug 2020.



Submit your article to this journal [↗](#)



Article views: 326



View related articles [↗](#)



View Crossmark data [↗](#)



Tailoring geometric phases of two-dimensional functional materials under light: a brief review

Jian Zhou

Center for Advancing Materials Performance from the Nanoscale, State Key Laboratory for Mechanical Behavior of Materials, Xi'an Jiaotong University, Xi'an, China

ABSTRACT

Information storage relies on the fast and reversible memory devices, which can read and write data easily with low energy input. In addition, in order to pursue high data storage density and miniaturizing device size, low-dimensional materials with large area to volume ratio would be preferable. Up to date, there are already a lot of explorations of two-dimensional functional material based devices with interesting phase transitions. According to Ginzburg-Landau theory, phase transition occurs when order parameter changes, under external stimuli such as temperature, electric field, or external stress. Other than these, novel phase transition mechanisms under *low-frequency* light irradiation has been recently proposed. The light frequency is below the corresponding energy bandgap of the semiconductors, which intuitively has very small scattering cross sections. However, according to thermodynamic theory, there could have light-matter interactions. Geometric structure can be changed and manipulated under light illumination. If ion displacements are strong enough, phase transition could occur. This optically driven phase transition approach requires no direct contacts with the sample, so that this procedure is easily controlled. In this mini-review, we briefly summarize the basic theory, computational predictions and some very recent experiments on low-frequency light induced phase transition in various systems.

ARTICLE HISTORY

Received 17 April 2020
Accepted 14 August 2020

KEYWORDS

Phase transition;
optomechanics; ferroelectric
materials; 2D materials

Introduction

The current century has already witnessed the unprecedented information explosion, especially during the past decade. This boosts the requirement to store information and data in ultraminiaturized electronic devices and the related technologies are also highly needed. From materials point of view, the currently used commercial information storage media is based on Ge-Sb-Te alloys (GST, such as GeSb_2Te_4 and $\text{Ge}_2\text{Sb}_2\text{Te}_5$) which could exist in at least two states [1]. Generally speaking, a GST alloy is in the length scale on the order of a few hundred nanometers to a few micrometers, and its ground state is a layered crystal, where Te anions form flat layers, and Ge/Sb cations are intercalated into two Te layers and serve as cement to stabilize Te layers. Upon laser irradiation, the system would absorb heat and transform its crystalline phase into a metastable amorphous structure, which has

CONTACT Jian Zhou jianzhou@xjtu.edu.cn Center for Advancing Materials Performance from the Nanoscale, State Key Laboratory for Mechanical Behavior of Materials, Xi'an Jiaotong University, Xi'an 710049 China

© 2020 The Author(s). Published by Informa UK Limited, trading as Taylor & Francis Group.

This is an Open Access article distributed under the terms of the Creative Commons Attribution License (<http://creativecommons.org/licenses/by/4.0/>), which permits unrestricted use, distribution, and reproduction in any medium, provided the original work is properly cited.

a much higher (several orders of difference) electric resistivity. Another few laser pulses could premelt the amorphous structure, and the system quenches back to its crystalline form. Thus, two structural phases with a giant contrast electric resistivity could be realized, which perform as '0' and '1' state in information storage and readout process [2].

The transformation in the crystalline-to-amorphous phase change process requires a large amount atoms moving long distances. This belongs to the diffusional phase transition, where the topology and environment around each atom change drastically before and after transformation. One could not find a clear diffusion pathway during phase change. From energy point of view, intuitively speaking, it requires a large amount of input energy to trigger melting. Hence, the phase change is sluggish (typically a few to a few hundred nanoseconds) and energy consuming. We know that atomic vibrational frequency is on the order of terahertz ($\text{THz} \sim 10^{12} \text{ s}^{-1}$), so that there still has a big room to reduce the phase transition timescale, from nanoseconds to picoseconds, once the amount of atomic displacement can be reduced on the order of unit cell length. Therefore, a natural question arises: if one can design some crystalline-to-crystalline phase transition materials, which require less energy input for data/information writing, yet possessing good contrast signal for information readout. One could imagine that such novel phase transition material would also greatly reduce waste heat during operation, if appropriate manipulating schemes can be designed. Since the atomic movement is diffusionless, good reversibility is easily guaranteed, with elongated device lifetime.

Phase transition is a long-standing problem that may cover most of physics researches [3]. It could be triggered by temperature, pressure, electric field, magnetic field, or optical field, etc. [4]. A material is composed by ions and its surrounding (valence) electrons. Thus, in the materials science, phase transition could occur either atomically or electronically, or both. For example, one famous electronic (without atomic movement) phase transition is ferromagnetic to paramagnetic transition, usually driven by varying temperature, which has been widely used in magnetic based memory and storage media [5]. Alternatively, atomic diffusionless phase change materials are receiving great attention during the past decade, as they are considered as next-generation information storage materials with low energy consumption and fast kinetics. In addition, due to the dramatic advances of fabricating atomically thin two-dimensional (2D) layered materials, 2D phase change materials are also attracting great attention, as they could enhance information storage density by several orders [6]. Up to now, there have been quite a lot of theoretical and experimental researches focusing on crystalline-to-crystalline diffusionless phase transitions of 2D materials under atomic impurity, mechanical, thermal, or electronic stimuli [7]. These works prove that geometries and phases of 2D functional materials can be well controlled, and suggest that their realistic applications in miniaturized devices will be promising in the near future.

In order to enhance the phase change kinetics of 2D functional materials, one has to resort to new schemes, rather than conventional strategies. This is because either mechanical or electronic approach needs direct mechanical or electrochemical contacts with samples, and such contacts may introduce unwanted impurities, stress, and charges. The additional interactions at the contacting interface also reduces the kinetics. Thermal stimulus requires to excite phonons of materials, and its transport speed is limited by the thermal conductivity. Therefore, to explore fast and noncontact phase change methods, one possible solution is to use light [8].

Interaction between light and dielectrics is different under different optical frequency. There are two characteristic frequencies separating the whole frequency regimes, namely, absorption frequency ω_0 , and plasmon frequency ω_p . When the optical frequency is below ω_0 , the optical absorption $\epsilon^{(2)}$ (and also conductivity σ) can be eliminated, leaving only dispersive effect of optics (finite real part of permittivity $\epsilon^{(1)}$). Around ω_0 (in between $(\omega_0 - 1/\tau)$ and $(\omega_0 + 1/\tau)$, where τ is electron lifetime), significant light absorption occurs so that photons excite electrons up to conduction bands (depending on the scattering cross section). Starting from $\omega_0 + 1/\tau$ and up to ω_p , there will be a strong optical reflection at the surface, so that most of light cannot go inside the material. However, since the 2D materials are usually in subnanometer thickness, the reflectance could be reduced, considering the characteristic in-depth length is usually in the range of a few to a few tens nanometers. After that ($> \omega_p$), the system is transparent to light. While a lot of theoretical and experimental studies focus on the second frequency regime (light absorption) [9,10], the recombination of ‘hot’ electrons and holes may produce too much waste heat through nonradiative process, which is also harmful to devices. Therefore, we will mainly discuss the first frequency regime, where no or very small portion of photons irradiated onto the material can be absorbed. In this mini-review, we will briefly summarize the very recent theory and experimental achievements in controlling some promising 2D functional material geometries by low-frequency optics field, and discuss some of future developments in this field. In these circumstances, we only consider the electric field feature of light, while the photon particle feature can be eliminated.

Thermodynamic theory

Light contains both alternating electric and magnetic field components. According to electromagnetic dynamics theory, the magnetic field interaction with materials is usually orders of magnitude smaller than that of electric field interaction. Hence, we will only focus on the effects of electric field, which can be written in the form of

$$\vec{\mathcal{E}} = \mathbf{E} \exp(i\omega t)$$

Here, \mathbf{E} is the electric field vector, and ω is optical frequency. Without loss of generality, we denote the field propagation direction to be z , which is the normal direction of 2D material surface. Since an alternating electric field in free space is a transverse field, \mathbf{E} only contains x and y components. For the x - (or y -) polarized linearly polarized light, \mathbf{E} takes the form of $(E_0, 0, 0)$ [or $(0, E_0, 0)$]. For left-handed (or right-handed) circularly polarized light, \mathbf{E} can be $(E_0, i \times E_0, 0)$ [or $(E_0, -i \times E_0, 0)$], where $i = \sqrt{-1}$. Note that here the electric field is alternating, which is naturally different from the static electric field that is produced by electrochemically patterned electrodes on the materials.

Under such alternating electric field, the electrons and ions in a material would be accelerated. If the system is under isothermic and isobaric boundary condition, the thermodynamic Gibbs free energy of the system can then be evaluated according to [11]

$$\mathcal{G}(\vec{\mathcal{E}}, \omega, t) = U - TS + pV - V \text{Re}(\vec{\mathcal{D}}^* \cdot \vec{\mathcal{E}})$$

where $\vec{\mathcal{D}}$ is electric induction of the system, U , T , S , p , and V are the internal energy, temperature, entropy, pressure, and total volume, respectively. In linear constructive

materials, the electric induction can be written as $\bar{\mathbf{D}} = \bar{\mathbf{D}}_0 + \epsilon_0 \bar{\bar{\epsilon}}(\omega) \mathbf{E}$, where $\bar{\bar{\epsilon}}$ is relative permittivity (dielectric) tensor. Thus, even without any photon absorption, the electric field component carried by the light also interacts with the material, as a function of the frequency-dependent dielectric function $\bar{\bar{\epsilon}}(\omega)$.

The Gibbs free energy, like internal energy in usual cases, is a thermodynamic averaged physical quantity. Under ergodic assumption, the ensemble average of $\mathcal{G}(\omega)$ is equivalent with time average. Thus, $\mathcal{G}(\omega) = \langle \mathcal{G}(\omega, t) \rangle$. In the following discussion, we will omit the $\langle \cdot \rangle$ notation, and time average is always taken. The time averaged Gibbs free energy is then

$$\mathcal{G}(\mathbf{E}, \omega, \bar{\bar{\epsilon}}^{(1)}) = U - TS + pV - V \epsilon_0 \mathbf{E} \cdot \bar{\bar{\epsilon}}^{(1)} \cdot \mathbf{E}$$

Note that in the above expression, we have neglected the spontaneous static electric induction $\bar{\mathbf{D}}_0$, as it is a zero frequency quantity and will be averaged out by long time integration.

Without light irradiation, the local equilibrium state (stable or metastable state) of a material satisfies equilibrium condition,

$$\partial \mathcal{G}(0, 0, \bar{\bar{\epsilon}}^{(1)}) / \partial u_i = 0,$$

$$\text{and } \partial^2 \mathcal{G}(0, 0, \bar{\bar{\epsilon}}^{(1)}) / \partial u_i \partial u_j > 0 \text{ (positively definite).}$$

This equilibrium condition needs to be modified once low-frequency light is illuminated, as the frequency dependent dielectric function is coordinate dependent as well,

$$\partial \mathcal{G}(\mathbf{E}, \omega, \bar{\bar{\epsilon}}^{(1)}(\omega, \{u_i\})) / \partial u_i = 0,$$

$$\text{and } \partial^2 \mathcal{G}(\mathbf{E}, \omega, \bar{\bar{\epsilon}}^{(1)}(\omega, \{u_i\})) / \partial u_i \partial u_j > 0.$$

Therefore, under light illumination, the equilibrium structure changes. Intuitively, since at the low-frequency region the real part of dielectric function is always positive, the system would always transit to the state with larger value of $\bar{\bar{\epsilon}}^{(1)}$ component under electric field. Once again, we do not assume significant photon absorption in the system, as such photon dissipation does not correspond to work done into materials. One could see a clear similarity between this light induced geometric variation and the optical tweezer technique – the latter also uses nonabsorption light matter interaction to move atoms or molecules. The light changing material geometry can then be considered as optical tweezer effect on the generalized reaction coordinate space, and the light matter interaction is changing the shape of potential energy landscape. We will illustrate this theory in the following theoretical studies with some promising 2D functional materials. Some very recent experimental achievements with noncontacting laser inducing phase transitions are then summarized.

Theoretical predictions of some 2D phase transition materials under light

One of the most studied structural phase transition materials is structural ferroic materials, including ferroelectric and ferroelastic orders. In a 2D structural ferroic material, below Curie temperature, there will be multidomains hosting different ferroelectric or ferroelastic phases. Even though different phases are generally structural equivalent (usually subject to a mirror or rotation operation), they could show different optical reflectivity under linearly polarized light, so that can be readout optically. The question is then if one can apply a laser pulse and drive different ferroic order transition. During the past few years, there have been quite a few novel 2D ferroelectric and ferroelastic materials theoretically predicted [12,13] and experimentally observed [14]. Some of them have intermediate energy barriers, providing good platforms to study and observe possible light induced phase transitions.

The first optically switchable material predicted theoretically was monolayer SnO, which is a recently discovered 2D ferroelastic material under low temperature [15]. Its high symmetric parental phase shows a square lattice, and could spontaneously reduce its symmetry and becomes rectangular lattices (ferroelasticity), orientating along the x - or y -direction. The goal would be to apply a laser pulse with selected frequency, intensity, and polarization direction to drive phase transition between different orientation variants (x -ferroelastic \leftrightarrow y -ferroelastic). Intuitively, one could choose linearly polarized light (LPL), as it breaks the spatial symmetry in the xy plane. If we denote the two orientation variants as FE1 and FE2, then their Gibbs free energies are degenerate before light is illuminated, $\mathcal{G}_{\text{FE1}}(0) = \mathcal{G}_{\text{FE2}}(0)$.

In order to evaluate the optical response, one could calculate the frequency-dependent dielectric function according to random phase approximation approach [16,17],

$$\bar{\epsilon} = 1 - \frac{e^2}{2\pi^2} \int d\mathbf{k} \sum_{c,v} \frac{\langle u_{v,\mathbf{k}} | \mathbf{k} | u_{c,\mathbf{k}} \rangle \langle u_{c,\mathbf{k}} | \mathbf{k} | u_{v,\mathbf{k}} \rangle}{E_{c,\mathbf{k}} - E_{v,\mathbf{k}} - \hbar\omega - i\xi}$$

Here $|u_{n,\mathbf{k}}$ and $E_{n,\mathbf{k}}$ are cell-periodic part of Bloch wavefunction and its eigenvalue of band- n at \mathbf{k} in the momentum space, respectively. Due to the broken of C_4 -symmetry, the light absorption (which corresponds to imaginary part of dielectric function) selectivity for the x - and y -LPL are different. According to Kramers-Kronig relation, the real part of dielectric function for the x - and y -LPL are also different, even below the optical bandgap [18]. This can be seen in Figure 1. One observes that the near band edge (NBE) optical responses of the FE1 and FE2 under x -LPL show a clear contrast. Therefore, under a laser illumination, the Gibbs free energies of the two orientation variants become nondegenerate,

$$\mathcal{G}_{\text{FE1}}(\omega) = \mathcal{G}_{\text{FE1}}(0) - \frac{1}{2} S_{\infty 0} \in_{\text{FE1}}^2 E^2 < \mathcal{G}_{\text{FE2}}(0) - \frac{1}{2} S_{\infty 0} \in_{\text{FE2}}^2 E^2 = \mathcal{G}_{\text{FE2}}(\omega)$$

This lifts the degeneracy of the two orientation variants, so that phase transition from FE2 (with higher Gibbs free energy) to FE1 (with lower Gibbs free energy) phase could occur thermodynamically. If one would like a transition from FE1 to FE2, then only a y -polarized LPL is needed. Note that the frequency selected is below the optical direct bandgap, then no electron excitation from valence to conduction band occurs – only pure mechanical response exists.

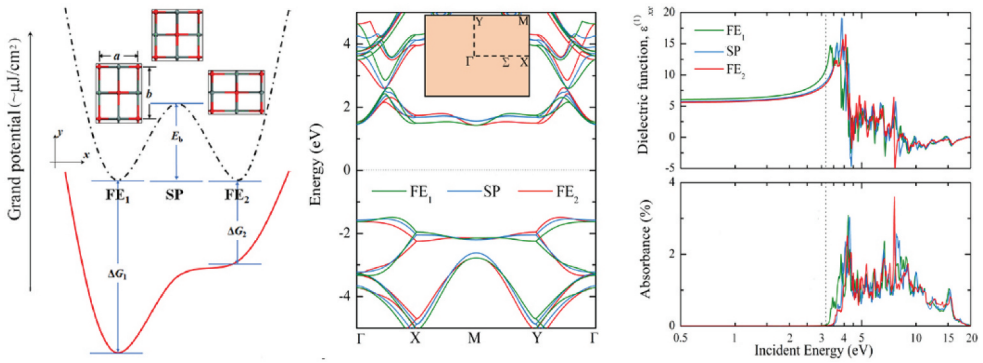


Figure 1. (Left panel) Elastic energy curve of degenerate FE1 and FE2 states (black dot dashed curve) without light irradiation. LPL lowers their Gibbs free energy and also lifts their degeneracy (red solid curve). (Middle panel) Band dispersions of FE1, saddle point (SP), and FE2 along high symmetry path in the first Brillouin zone. (Right panel) Real part dielectric function $\epsilon_{xx}^{(1)}$ and optical absorption spectra calculated according to RPA. The dashed vertical line denotes NBE optical energy $\hbar \omega_0 = 3.25$ eV. Figure adapted from [18].

The phase transition kinetics can be simply evaluated. Through DFT calculation, the phase transition saddle point corresponds to the square lattice structure, with an energy barrier of 0.6 meV per formula unit (f.u.), separating the two ferroic orientation variants. If the saddle point Gibbs free energy is also included, one would find a critical field magnitude value, above which the Gibbs free energy barrier *disappears*. This corresponds to a barrier-free phase transition. According to the Arrhenius reaction law $\kappa = \nu_0 e^{-E_b/k_B T}$, where κ is the reaction frequency [19], vanishing of energy barrier indicates an ultrafast phase transition which is governed by the trivial frequency ν_0 . Since the ion frequency is on the order of terahertz, then the phase transition should occur on the order of picoseconds as well. Comparing with diffusional phase change in GST alloys which usually occurs on the order of a few to a few hundred nanoseconds, this diffusionless martensitic barrier-free phase transition could drastically reduce the operation time. In addition, the phase transition kinetics could avoid the conventional nucleation and growth process, and occurs everywhere light is irradiated.

To read the ferroic order information, one could measure their reflectivity under LPL. The reflectivity of a perpendicular incident light can be calculated by $R = \frac{(n-1)^2}{(n+1)^2}$, where n is the refractive index $n = \text{Re} \epsilon^{1/2}$. This also provides a damage-free measurement approach, ensuring the good reversibility of the devices.

More examples can be provided. Figure 2 shows a time-reversal invariant multiferroic material, monolayer SnSe, which possesses both ferroelectric and ferroelastic orders simultaneously [20,21]. The optical response functions of two orientation variants of SnSe also show a large contrast at the incident energy of $\hbar \omega_0 = 0.96$ eV. If a y-polarized LPL pulse is illuminated, a phase transition from FE1 to FE2 could happen. Of course an x-polarized LPL could trigger FE2 to FE1 phase transition. In a monolayer SnSe, the transition saddle point lies 1.76 meV above the ferroic structure, indicating a larger energy barrier than that in the monolayer SnO. The critical field magnitude of barrier-free phase

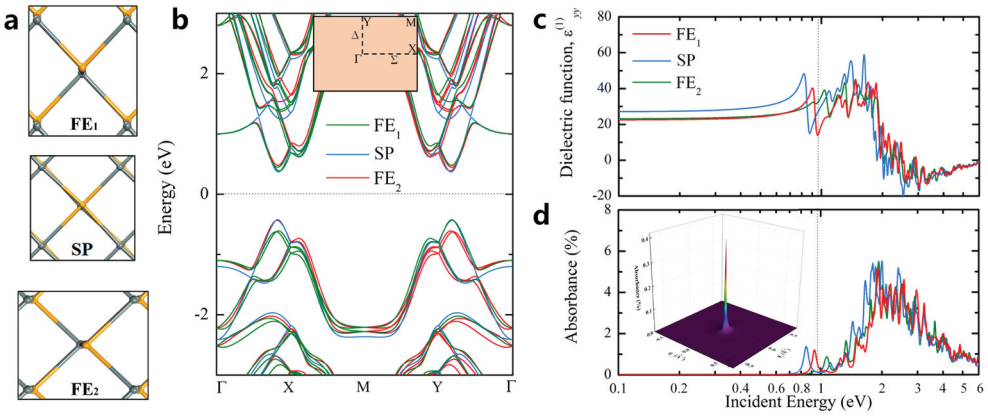


Figure 2. (a) The geometric structures of a SnSe monolayer in FE1, FE2, and SP states. (b) Band dispersions along the high symmetric k -path. Inset shows the first Brillouin zone of FE1 orientation variant. (c) Real part dielectric function $\epsilon_{yy}^{(1)}$ of different states. (d) Optical absorbance spectra. The vertical dashed line denotes an incident energy of 0.963 eV. Inset of (d) shows the absorbance of FE1 in the whole k -space. Figure adapted from [18].

transition is evaluated to be 0.29 V/nm (corresponding to intensity of 1.2×10^{10} W/cm²). This is an intermediate intensity that can be achieved in the laboratory. Phase transformation between topologically trivial SnSe phase ($Pnma$ space group) and nontrivial phase $Fm-3m$ can also be triggered under light [22]. Similar approach in a single element ferroelastic and ferroelectric monolayer Bi(110) is also proposed [23].

Not only ferroic order switch in ferroics, one can also use LPL to drive phase transformation. For example, when two h-BN sheets stack together, they could stay at various stacking patterns [24,25]. Figure 3 shows three typical stacking patterns [26]. First-principles calculations suggest that the AA' pattern is the ground state of h-BN bilayer, while the AB' pattern is a metastable state, energetically higher than the AA' by 2 meV/f.u. (f.u. indicates formula unit). The A'B pattern is energetically much higher, which usually does not occur under ambient condition. One could imagine that these different stacking patterns can be realized by translating or sliding the top layer with respect to the bottom layer, measured by a displacement variable u . Similar procedure can be applied to this system. The real part of dielectric function depending on u and ω is plotted in Figure 3. One can see that if the incident energy $\hbar\omega$ is selected at 4.30 eV, then the real part of dielectric function for the AB' pattern is larger than that of the AA' pattern. Hence, a laser with photon energy of 4.30 eV could translate the AA' ground state into metastable AB'.

One could apply a simple 1D atomic chain model to semiempirically evaluate the phase transformation kinetics. Denoting the n -th cell displacement as u_n , then the equation of motion is [26]

$$\frac{\partial^2 u_n}{\partial t^2} = \frac{\kappa}{m}(u_{n+1} + u_{n-1} - 2u_n) - \frac{1}{ma^2} \left[\frac{\partial U_{\text{vdW}}(u_n)}{\partial u_n} - \frac{\epsilon_0 V E^2(n)}{2} \frac{\partial \epsilon(u_n)}{\partial u_n} \right] - \gamma \frac{\partial u_n}{\partial t}$$

Here m is the effective mass, κ is elastic lattice constant, a is lattice parameter, γ is a phonon-phonon scattering damping term. van der Waals interaction U_{vdW} is also included. The simulation was done by using 20,000 unit cells ($n = 1, 2, \dots, 20,000$) in 1D

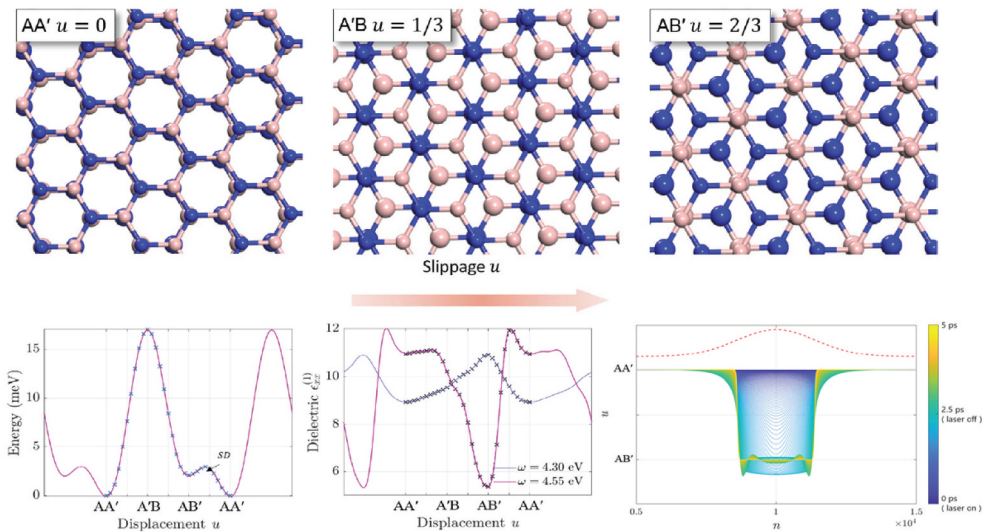


Figure 3. (Up panel) Three high symmetry stacking modes AA', A'B' and AB' of h-BN bilayer. They are different by a translational sliding variable u along the armchair direction (red arrow). (Lower left) Intrinsic Gibbs free energy landscape. (Lower middle) Calculated dielectric function at an incident optical energy of 4.30 to 4.55 eV. (Lower right) Dynamics of the model system under different laser illumination. Writing AB' domain. Initially the system is in a homogeneous AA' stacking mode. From $t = 0$ to 2.5 ps, laser of photon energy 4.3 eV is used, which favors AB' stacking mode shines on the middle region. An AB' domain gradually develops. The dashed curve above shows Gaussian beam laser profile. After several oscillations, middle region of the system is locked in the AB' stacking mode. Figure adapted from [26].

under a Gaussian beam laser $E(n) = E_0 \exp\left(-\frac{(n-n_0)^2}{2\sigma^2}\right)$, with $E_0 = 5$ V/nm, $n_0 = 10,000$, and $\sigma = 2000$ (full width at half maximum ~ 1 μm). The result is shown in Figure 3 (lower right panel). Starting from AA', one shines a laser of $\hbar\omega = 4.3$ eV near the center. After 2.5 ps, the laser is turned off, and the system is allowed to relax. At 5 ps, the laser illuminated AA' transforms to AB', demonstrating an ultrafast (picosecond time scale) phase transformation kinetics. If one tunes the laser frequency to $\hbar\omega = 4.55$ eV, AB' could quickly transforms back to AA'. A schematic 2D recording device can then be proposed, as shown in Figure 4. Each patch is an h-BN bilayer, which could exist in AA' or AB' pattern. A laser moves to read and write structural information, which not only triggers phase transformation, but also read the bilayer pattern by measuring its reflectivity. Due to the optical diffraction limit, the size of each patch should exceed 300 nm.

Experimental observations of phase transition under low-frequency light

The low-frequency (below optical bandgap) light driven phase transition has already been observed experimentally during recent years. In 2018, Rubio-Marcos *et al.* studied the optically driven phase domain movement in a well-known perovskite, BaTiO₃ (BTO) [27], as shown Figure 5. Even though the BTO has a fruitful different phases under different pressure and temperature, the authors performed their experiments under room

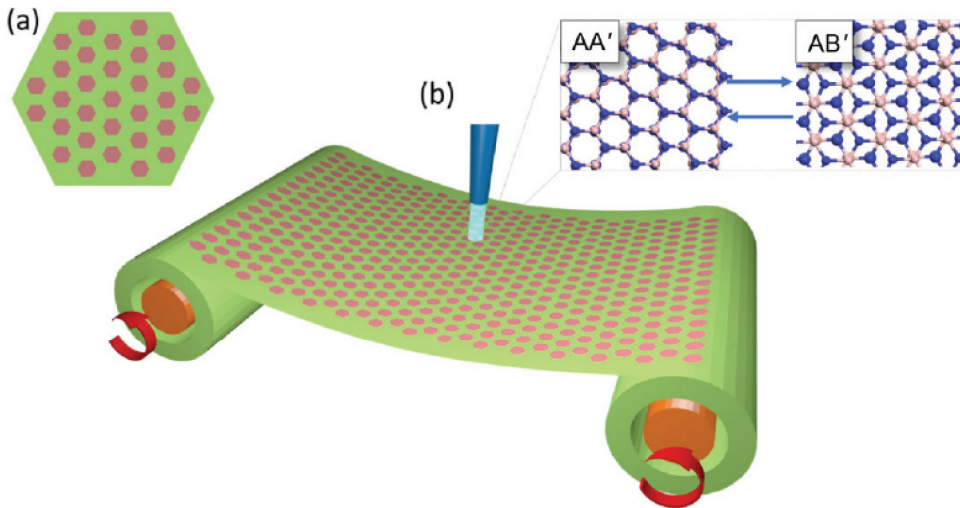


Figure 4. (a) Hexagons represent bilayer h-BN. They are separated with each other, so that no interactions exist between different patches. (b) An optical disk drive composed by a lattice of bilayer h-BN sheets. Inset shows two typical patterns. Figure adapted from [26].

temperature, and BTO shows a tetragonal phase with its spontaneous polarization pointing along the elongated direction, $\langle 001 \rangle$. In experiments, the BTO crystal usually forms multidomains with the polarizations pointing along perpendicular to or parallel with the surface normal direction. They are termed as '*a*-domain' and '*c*-domain,' respectively. The boundary is referred to as '*b*-domain,' which also consists multiple microscale polarization structures. Rubio-Marcos *et al.* used a laser with its wavelength of 532 nm (corresponding to 2.3 eV, which is about 2/3 of the BTO bandgap) to illuminate onto the system. Even though there is no electron excited from the valence band to conduction band, the system is still excited, with the domain boundary (*b*) emerging between the *a*- and *c*-domain. This indicates that, under low-frequency light shining, the *a*-domain could flip its polarization direction out-of-plane, and a phase transition of *a* to *b* and *c* could occur. This is also demonstrated from their synchrotron radiation ($\lambda = 0.5636 \text{ \AA}$) high resolution X-ray radiation diffraction measurement. Once the light is turned off, the residue resilient stress drives the domain boundary back to its original position. Hence, this phase transition is reversible but volatile. This is partially because the BTO sample is too thick and the transition is not complete. Their later experiment further shows the linear relation between light intensity and the transition extent [28].

Besides BTO which has a rotation of polarization axis, two individual groups focused on SrTiO_3 (STO) which has a more complicated phase diagram. The low temperature STO is also ferroelectric. However, as the temperature is lowered sufficiently, the quantum tunneling effect (zero temperature energy) becomes significantly, and the system shows paraelectric character. This is termed as quantum paraelectricity [29]. In 2019, two back-to-back papers published in Science reported their experimental observations of a 'hidden' phase at low temperature, when the STO is illuminated under terahertz laser [30,31]. They use terahertz laser, which could excite the phonon (ionic system) of STO, and the quantum paraelectric STO undergoes a phase transformation and becomes

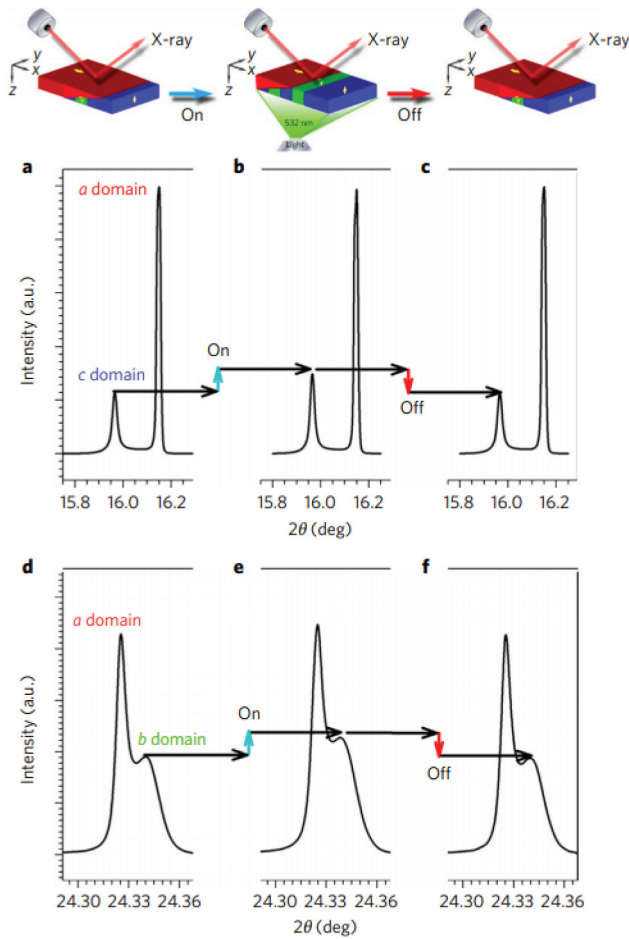


Figure 5. (a–c) Sequence of synchrotron radiation ($\lambda = 0.5636 \text{ \AA}$) high resolution XRD patterns. The red and blue regions represent *a* and *c*-domains, respectively. The contribution of the *c* domains enhances when the light is on. The optically induced change in the domain structure disappears after the light is switched off. (d–f) Sequence of XRD patterns of (300)/(030) reflections showing that the contribution of the *b* domains emerges after the light is switched on. Figure from [27].

ferroelectric without an inversion symmetry. The second harmonic generation measurements clearly demonstrate such phase change. Since this phase cannot be observed in conventional p - T phase diagram, it is a hidden phase that only appears under finite alternating electric field \mathbf{E} with selective frequency and intensity. Unfortunately, the exact ferroelectric atomic structure is still unknown (Figure 6).

These unprecedented discoveries suggest that optics can serve as an additional tuning parameter to explore larger phase diagram of materials. Actually, if one looks at the thermodynamics theory, the conventional Gibbs free energy contains two natural variables, p and T . These are the two axes of the phase diagram that we usually apply. When the optical electric field (and perhaps magnetic field) is added, it appears in the Gibbs free energy expression as additional natural variable. As we stated before, the equilibrium condition changes because the optical responses are also functions of coordinates $\{\mathbf{u}_i\}$.

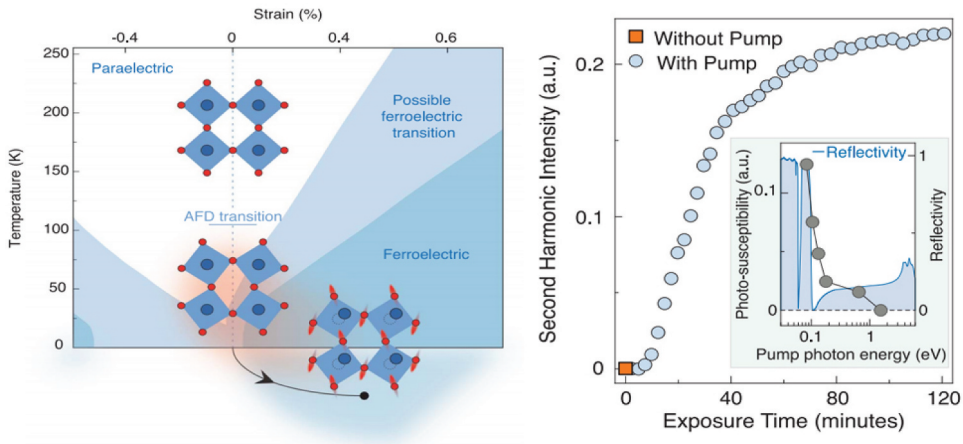


Figure 6. Dynamical ferroelectricity in SrTiO₃. Time delay-independent total second harmonic intensity impinging on the detector (without analyzer) as a function of exposure time to 15- μ m pump pulses. (Inset) Pump wavelength dependence. Figure from [30].

Hence, the field exerted force drives the structure to find new local minimum in the reaction coordinate space, showing new hidden phases. Remarkably, if the new phase is metastable in the p - T diagram, then it could exist even when the light is turned off, realizing nonvolatile phase transition.

For 2D materials, such light driven phase transformation is also seen experimentally. One of the most famous examples that attracts great attention recently is monolayer transition metal dichalcogenide (TMD). The phase transition of TMD monolayers is very promising, as they usually show two phases, namely, 2 H and 1 T'. Both of them are of significant importance with promising physical properties. The 2 H phase has an intermediate band-gap, with low energy bands lie at the K and K' points of the first Brillouin zone [32]. Owing to the inversion symmetry breaking, the electron states at these two points (electronic valleys) can be selectively excited by different handed circularly polarized light [33]. Thus, 2 H TMD can serve as a good valleytronic platform in the future, for very low energy consumption information storage devices. On the other hand, the 1 T' TMD monolayer is typically a semimetal, with inversion symmetry. It has two Dirac points in the first Brillouin zone, which can open a finite bandgap once spin orbit coupling is included. It thus is classified as a 2D Z_2 topological insulator, which hosts fault-tolerant quantum spin Hall effect and is applicable in future quantum computing devices [34]. From geometric point of view, the phase transformation between 2 H and 1 T' in TMD only involves a short distance sliding of one layer chalcogen atoms and a subsequent spontaneous M-M dimerization (Peierls distortion). Thus, it is also a martensitic phase transition with diffusionless atomic motions, and may occur ultrafast in a short timescale [35]. Several strategies have been proposed to induce phase transitions from the ground state 2 H to metastable 1 T' phase (except for monolayer WTe₂ whose 1 T' is energetically lower than 2 H), especially in the MoTe₂, as the two phases in this system differ least than other analogues.

A prior work was done by Kan *et al.*, who predicted that Li impurity can flip the relative energy difference between them [36]. Once the Li concentration exceeds a critical value, the 2 H structure has higher energy than the 1 T', and phase transition could occur

thermodynamically. Later on, it was realized that the Li effect is introducing electrons into the system, so external carrier doping can also do the work. E. Reed and his coworkers thus predicted gate voltage induced phase transition, which essentially changes the charging state of the system [37]. During charging, the system is exerted a strong in-plane stress. Li *et al.* unraveled that it is the strain that could fundamentally drives phase transition from 2 H to 1 T', and even among different 1 T' phase domains [35]. Experimentally, X. Zhang's group carried out the gating method and observe 2 H to 1 T' topological phase transition in MoTe₂ [38]. Later on, various experimental works also demonstrated such topological phase transition via vacancy engineering, or chemical doping.

Considering large optical response contrasts in the topologically trivial and nontrivial phases [39], one could imagine that light can be applied to drive fascinating topological phase transitions. Very recently, Shi *et al.* performed a careful experiment and showed that the 2 H phase of MoTe₂ can irreversibly transform to 1 T' under terahertz optics, demonstrating optically driven topological phase transition [40]. They generated ~0.3 MV/cm free-space THz fields which were strengthened to ~20–50 times using simple field enhancement structures consisting of 100 μm-wide parallel gold strips. Before THz irradiation, Raman spectroscopy shows two characteristic peaks, out-of-plane A_{1g} mode and in-plane E_{2g} mode. Then they irradiated the sample with five THz pulses whose field strength in free space was 270 kV/cm (and then field enhanced), these two peaks disappear and a new peak emerges at 163.3 cm⁻¹. This is the A_g Raman mode of the monolayer 1 T'-MoTe₂ phase. This peak can be furthermore strengthened after more pulses are irradiated. Such phase transition is also demonstrated via second harmonic generation measurement. After phase transition to 1 T', the sample did not transform back to 2 H, indicating an irreversible and permanent phase transition (Figure 7).

Another topological phase transition that could occur with small energy input relies on the different stacking patterns of WTe₂, which could exist in both T' and T_d phases [41,42]. They used crystallographic measurements and demonstrated that terahertz light pulses can induce terahertz-frequency interlayer shear strain with large strain amplitude in the Weyl semimetal WTe₂, leading to a topologically distinct metastable phase (ground state T_d phases to metastable T') [43]. The T_d phase is inversion asymmetric, which shows a pair of Weyl points (topological charges of $\chi_1 = 1$ and $\chi_2 = -1$) in the Brillouin zone, connected by a Fermi arc on the surface state. Under terahertz driven phase transition, the induced shear strain could linearly tune Weyl fermion distance in the momentum space $\mathbf{p} \rightarrow (\mathbf{p} - \chi e\mathbf{A})$, where e is the electron charge and \mathbf{A} is the gauge-field vector potential. After phase transition occurs, the two Weyl points (with opposite chirality) combine together and extinguish, since the T' phase is centrosymmetric. Second harmonic generation experiments are also carried out to confirm the transition.

Optically driven strain engineering

Even though the light intensity may not be strong enough to trigger a phase transition, it could affect the equilibrium position of the system on the potential landscape and some structural changes may occur. This corresponds to an elastic deformation of the material, and is usually termed as photostriction effect. The above bandgap optical illumination has already proved to apply strains into the systems, from experimental [44,45] and

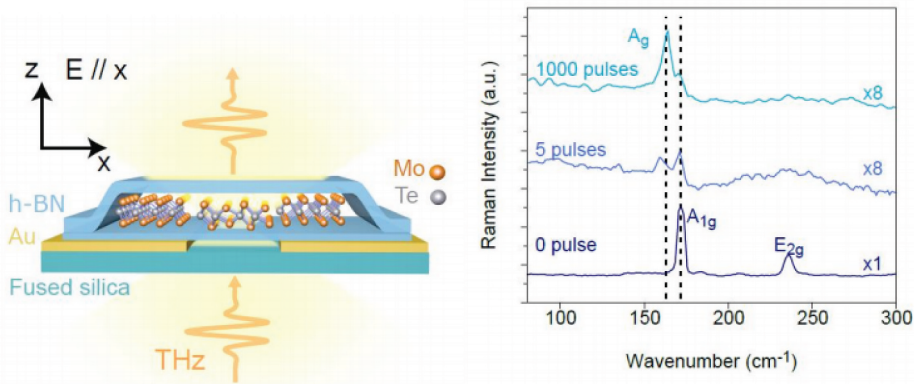


Figure 7. (Left panel) Structural illustration of monolayer 2 H-phase MoTe₂. THz pulses are incident from the fused silica substrate side. (Right panel) Raman spectra of monolayer MoTe₂ after THz pulse irradiation of 270 kV/cm. The A_g mode is at 163.5 cm⁻¹, characteristic of 1T' MoTe₂, appears clearly after 5 THz pulses and grows in further upon further irradiation, while the A_{1g} and E_{2g} modes of 2 H-MoTe₂ at 171.5 cm⁻¹ and 236 cm⁻¹ are strongly reduced. Figure from [40].

theoretical [46] evidences. The above bandgap light effect is mainly to excite electrons from the valence band to conduction band, generating electron-hole pairs (or excitons) in the system. Then, a combination of positively and negatively charged carriers change the geometry of materials, yielding photostriction effect.

If one uses light with its frequency below the semiconductor bandgaps, then the alternating electric field effect dominates. The previously mentioned Gibbs free energy analysis still holds, and the material could exert an elastic deformation as well. For example, an intermediate intensity light (with its frequency below direct optical absorption bandgap) irradiation can induce a large anisotropic compressive and tensile strain in 2D 1T' TMD monolayers [47] (Figure 8(a)). This is different from photostriction where photons are absorbed, hence we termed it as 'optostriction.' According to a simple dimensionality analysis, one could see that the optostrictive strain of the material is proportional to the intensity of light that irradiated onto it. The compressive strain here is an intrinsic elastic deformation, which does not suffer from Euler's buckling instability in conventional loading effects. Since usually the light has a spatial intensity gradient, it naturally generates a spatial strain gradient (Figure 8(b)). According to flexoelectricity theory, spatial strain gradient always produces polarizations. Thus, an in-plane optoflexoelectricity effect can be expected, which compensates the usual out-of-plane flexoelectricity effects by bending thin films. If such elastic deformation is strong enough to enter the plastic deformation regime, a phase transition could occur, as discussed previously.

Conclusion and Outlook

In this mini-review, we briefly introduce some recent developments of the phase transition and phase transformation under low-frequency light irradiation of 2D materials. Ferroic order switch and topological phase transition can occur under light with carefully selected frequency, intensity and polarization angle. Fast phase transition kinetics can be

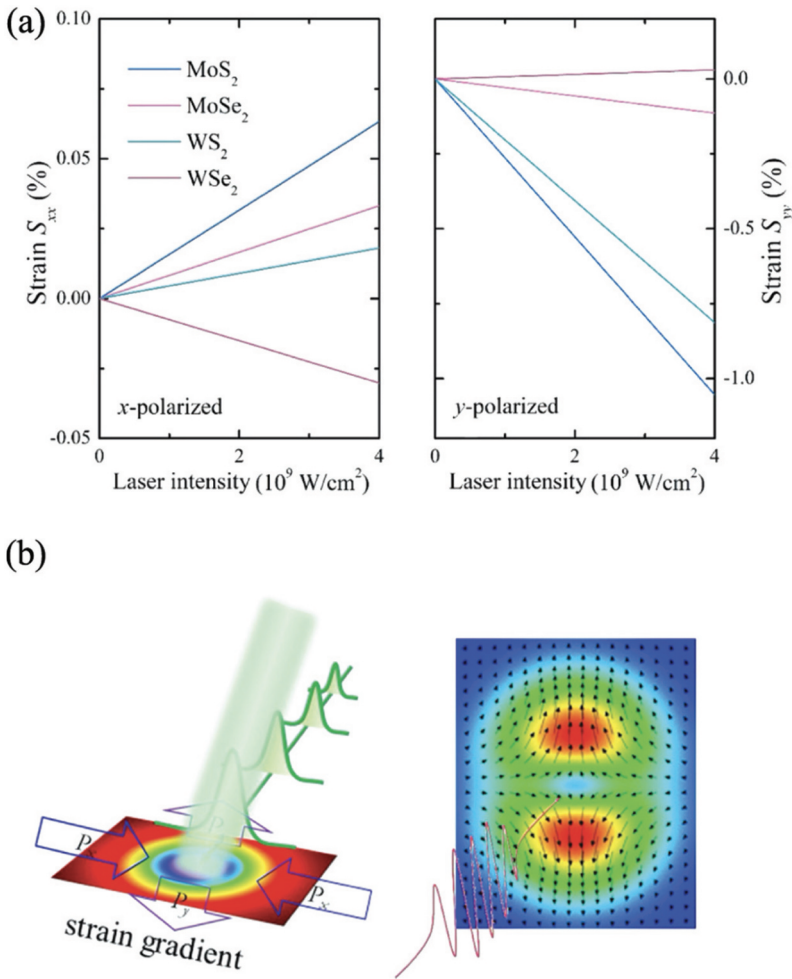


Figure 8. (a) Variation of uniaxial strain (along x and y direction) under (x and y polarized) laser. (b) Schematics of a Gaussian beam laser triggered strain gradient with optoflexoelectric polarization (hollow arrows). Right panel shows a 2D plot of strain gradient (colormap) and optoflexoelectric polarization texture (arrows). Figure adapted from [47].

expected once energy barrier can be overcome under optical illumination. The mechanism is similar as optical tweezer technique that applied in molecular physics and biology, which drives them moving in real space. The phase transition is also an optical tweezing effect of 2D materials in the generalized reaction coordinate space. From a dynamic point of view, the alternating electric field exerts time-periodic forces onto ions and/or electrons in the crystal, so that the Hamiltonian and dynamic force constant matrix become time dependent. According the Floquet theory, there would exist perturbations (Floquet energy levels) in addition to original static system. We anticipate that this nonvolatile, ultrafast, and facile phase transition mechanism in 2D materials can be applicable in the future nanoelectronic devices.

Disclosure statement

No potential conflict of interest was reported by the author.

Funding

This work was supported by the National Key Research and Development Program (Grant No. 2019YFA0210600), the National Natural Science Foundation of China under Grant Nos. 21903063 and 11974270, and the Young Talent Startup Program of Xi'an Jiaotong University.

ORCID

Jian Zhou  <http://orcid.org/0000-0002-2606-4833>

References

- [1] Zhang W, Mazzarello R, Wuttig M, et al. Designing crystallization in phase-change materials for universal memory and neuro-inspired computing. *Nat Rev Mater*. 2019;4:150.
- [2] Wuttig M, Lüsebrink D, Wamwangi D, et al. The role of vacancies and local distortions in the design of new phase-change materials. *Nat Mater*. 2007;6:122–128.
- [3] Lifshitz EM, Pitaevskii LP. *Physical kinetics*. Oxford, United Kingdom: Pergamon Press; 1981.
- [4] Brout R. *Phase Transitions*. New York, Amsterdam: W. A. Benjamin, Inc; 1965.
- [5] Kittel C. *Introduction to solid state physics*. 6th ed. Hoboken, New Jersey: John Wiley & Sons; 1986.
- [6] Duan X, Xu Y. The blossoming of 2D materials. *Acta Phys Chim Sin*. 2019;35:1039.
- [7] Wang X, Song Z, Wen W, et al. Potential 2D materials with phase transitions: structure, synthesis, and device applications. *Adv Mater*. 2019;31:1804682.
- [8] Yeats AL, Pan Y, Richardella A, et al. Persistent optical gating of a topological insulator. *Sci Adv*. 2015;1:e1500640.
- [9] Chen N-K, Li X-B. Unconventional phase transition of phase-change-memory materials for optical data storage. *Chin Phys B*. 2019;28:104202.
- [10] Chen N-K, Li X-B, Bang J, et al. Directional forces by momentumless excitation and order-to-order transition in peierls-distorted solids: the case of GeTe. *Phys Rev Lett*. 2018;120:185701.
- [11] Landau LD, Lifshitz EM, Pitaevskii LP. *Electrodynamics of continuous media*. 2nd ed., Vol. 8., Oxford, United Kingdom: Butterworth-Heinemann; 1984.
- [12] Wu M, Jena P. The rise of two-dimensional van der Waals ferroelectrics. *Wiley Interdiscip Rev Comput Mol Sci*. 2018;8(5):e1365.
- [13] Yang Q, We M, Li J. Origin of two-dimensional vertical ferroelectricity in WTe₂ bilayer and multilayer. *J Phys Chem Lett*. 2018;9:7160.
- [14] Xiao J, Wang Y, Wang H, et al. *Nat Phys*. 2020. DOI:10.1038/s41567-020-0947-0
- [15] Seixas L, Rodin AS, Carvalho A, et al. Multiferroic two-dimensional materials. *Phys Rev Lett*. 2016;116:206803.
- [16] Gajdoš M, Hummer K, Kresse G, et al. Linear optical properties in the projector-augmented wave methodology. *Phys Rev B*. 2006;73:045112.
- [17] Shung -KW-K. Dielectric function and plasmon structure of stage-1 intercalated graphite. *Phys Rev B*. 1986;34:979.
- [18] Zhou J, Xu H, Li Y, et al. Opto-mechanics driven fast martensitic transition in two-dimensional materials. *Nano Lett*. 2018;18:7794.
- [19] Arrhenius SA. "Über die Reaktionsgeschwindigkeit bei der Inversion von Rohrzucker durch Säuren. *Z Phys Chem*. 1889;4:226.
- [20] Wu M, Zeng XC. Intrinsic ferroelasticity and/or multiferroicity in two-dimensional phosphorene and phosphorene analogues. *Nano Lett*. 2016;16:3236.

- [21] Fei R, Kang W, Yang L. Ferroelectricity and Phase Transitions In Monolayer Group-IV monochalcogenides. *Phys Rev Lett.* **2016**;117:097601.
- [22] Zhou J, Zhang S, Li J. Normal-to-topological insulator martensitic phase transition in group-IV monochalcogenides driven by light. *NPG Asia Mater.* **2020**;12:2.
- [23] Pan Y, Zhou J. Toggling valley-spin locking and nonlinear optical properties of single-element multiferroic monolayers via light. *Phys Rev Appl.* **2020**;14:014024.
- [24] Marom N, Bernstein J, Garel J, et al. Stacking and registry effects in layered materials: the case of hexagonal boron nitride. *Phys Rev Lett.* **2010**;105:046801.
- [25] Constantinescu G, Kuc A, Heine T. Stacking in bulk and bilayer hexagonal boron nitride. *Phys Rev Lett.* **2013**;111:036104.
- [26] Xu H, Zhou J, Li Y, et al. Optomechanical control of stacking patterns of h-BN bilayer. *Nano Res.* **2019**;12:2634.
- [27] Rubio-Marcos F, Ochoa DA, Del Campo A, et al. Reversible optical control of macroscopic polarization in ferroelectrics. *Nat Photon.* **2018**;12:29.
- [28] Paez-Margarit D, Rubio-Marcos F, Ochoa DA, et al. Light-Induced capacitance tunability in ferroelectric crystals. *ACS Appl Mater Inter.* **2018**;10:21804.
- [29] Müller KA, Burkhard H. SrTiO₃: an intrinsic quantum paraelectric below 4 K. *Phys Rev B.* **1979**;19:3593.
- [30] Nova TF, Disa AS, Fechner M, et al. Metastable ferroelectricity in optically strained SrTiO₃. *Science.* **2019**;364:1075.
- [31] Li X, Qiu T, Zhang J, et al. Terahertz field-induced ferroelectricity in quantum paraelectric SrTiO₃. *Science.* **2019**;364:1079.
- [32] Xiao D, Liu G-B, Feng W, et al. Coupled spin and valley physics in monolayers of MoS₂ and other group-VI dichalcogenides. *Phys Rev Lett.* **2012**;108:196802.
- [33] Cao T, Wang G, Han W, et al. Valley-selective circular dichroism of monolayer molybdenum disulphide. *Nat Commun.* **2012**;3:887.
- [34] Qian X, Liu J, Fu L, et al. Quantum spin hall effect in two-dimensional transition metal dichalcogenides. *Science.* **2014**;346:1344.
- [35] Li W, Li J. Ferroelasticity and domain physics in two-dimensional transition metal dichalcogenide monolayers. *Nat Commun.* **2016**;8:10843.
- [36] Kan M, Wang JY, Li XW, et al. Structures and phase transition of a MoS₂ monolayer. *J Phys Chem C.* **2014**;118:1515.
- [37] Li Y, Duerloo K-AN, Wauson K, et al. Structural semiconductor-to-semimetal phase transition in two-dimensional materials induced by electrostatic gating. *Nat Commun.* **2016**;7:10671.
- [38] Wang Y, Xiao J, Zhu H, et al. Structural phase transition in monolayer MoTe₂ driven by electrostatic doping. *Nature.* **2017**;550:487.
- [39] Xu H, Zhou J, Wang H, et al. Giant photonic response of mexican-hat topological semiconductors for mid-infrared to terahertz applications. *J Phys Chem Lett.* **2020**;11:6119.
- [40] Shi J, Bie Y-Q, Chen W, et al. Terahertz-driven irreversible topological phase transition in two-dimensional MoTe₂. *arXiv:1910.13609.*
- [41] Li P, Wen Y, He X, et al. Evidence for topological type-II Weyl semimetal WTe₂. *Nat Commun.* **2017**;8:2150.
- [42] Lin CL, Arafune R, Liu R-Y, et al. Visualizing type-II weyl points in tungsten ditelluride by quasiparticle interference. *ACS Nano.* **2017**;11:11459.
- [43] Sie EJ, Nyby CM, Pemmaraju CD, et al. An ultrafast symmetry switch in a Weyl semimetal. *Nature.* **2019**;565:61.
- [44] Wen H, Chen P, Cosgriff MP, et al. Electronic origin of ultrafast photoinduced strain in BiFeO₃. *Phys Rev Lett.* **2013**;110:037601.
- [45] Kundys B, Viret M, Colson D, et al. Light-induced size changes in BiFeO₃ crystals. *Nat Mater.* **2010**;9:803.
- [46] Hu H, Liu M, Wang ZF, et al. Quantum electronic stress: density-functional-theory formulation and physical manifestation. *Phys Rev Lett.* **2012**;109:055501.
- [47] Zhou J, Mao S, Zhang S. Noncontacting optostriction driven anisotropic and inhomogeneous strain in two-dimensional materials. *Phys Rev Res (Rapid Commun).* **2020**;2:022059.